Electrical Power and Energy Systems 155 (2024) 109560

Contents lists available at ScienceDirect

International Journal of Electrical Power and Energy Systems

journal homepage: www.elsevier.com/locate/ijepes

Day-ahead energy-mix proportion for the secure operation of renewable energy-dominated power system

Ashish Shrestha [a,*], Yaju Rajbhandari [b], Francisco Gonzalez-Longatt [a,**]

[a] Department of Electrical Engineering, Information Technology and Cybernetics, University of South-Eastern Norway, Porsgrunn N-3918, Norway
[b] Department of Electrical and Electronics Engineering, Kathmandu University, Dhulikhel 45200, Nepal

ARTICLE INFO

Keywords:
Data-driven approach
Inverter-based resources
Power system dynamics
Renewable energy sources

ABSTRACT

Advancements in various scientific fields have encouraged the development of novel tools, techniques, components, methodologies, and innovations aimed at addressing the challenges encountered in modern power systems dominated by inverter-based resources (IBRs). This paper focuses on a concept that leverages historical time-series data obtained from transmission system operators (TSOs) to enhance the secure management and operation of power systems. By employing a data-driven model, the day-ahead values of power generation and load consumption are estimated and integrated with a dynamic model of the power system for further analysis. To optimize energy generation and ensure grid stability, an energy-mix operation and reserve scheduling model is utilized. This model optimally combines different power-generating technologies, including synchronous generators (SGs), grid-following converters (GFLs), and grid-forming converters (GFMs), to meet the energy demands of the day while enhancing the overall system strength. The findings are supported by quantitative analysis utilizing variables such as frequency, power production, terminal voltages, and system non-synchronous penetration (SNSP). Simulation results demonstrate that implementing the proposed concept enables the power system under consideration to operate securely, even in the face of a 38% increase in immediate load, with a maximum SNSP ratio of 59%. These findings highlight the effectiveness of the proposed approach in addressing the reliability, system dynamics, stability, control efficiency, and security challenges posed by IBR-dominated power systems. Furthermore, it is believed that this research contributes to the ongoing efforts in decarbonization, renewable energy integration, and combating global warming by facilitating the secure and optimized operation of renewable energy-dominated power systems.

1. Introduction

As people's knowledge of environmental issues and concerns about sustainability, renewable energy sources (RESs) have witnessed a rise in popularity in recent years. Due to environmental concerns and technological advancement, most countries are incorporating RESs into their grid and planning to make them 100% renewable [1]. The 26th United Nations Climate Change Conference (COP26) was kicked off on 1st November 2021 and mentioned different actions that should be conducted as soon as possible [2]. The major objectives of that conference were: (a) secure global net-zero emissions by mid-century, (b) keep 1.5 °C of global warming compared with pre-industrial levels within reach, (c) commit to mobilizing USD 100 billion per year by 2025 to help developing countries deal with the adverse effects of climate change, and (d) finalize the set of rules guiding the implementation of the Paris Agreement [2]. These objectives show the interest in renewable energy and RES-based power systems in the current era.

However, there are a lot of issues that should be discussed while talking about the RES-based power system. Reliability, system dynamics, stability, control efficiency, security, and other associated concerns [3], are among the most significant technical challenges faced by the RES industry. Studies [4,5], discussed that the increased usage of power electronic converter (PEC)-based RES complicates the power grid, and may affect the overall performance. The high penetration of PEC-based energy resources, such as wind turbines and solar PV, reduces the system's inertia. As a result of the low inertia of PEC-based technologies, the crucial fault clearance time is drastically shortened [6,7]. These complexities can also contribute to the instability of the power

* Corresponding author.
** Corresponding author.
E-mail addresses: Ashish.Shrestha@usn.no (A. Shrestha), fglongatt@fglongatt.org (F. Gonzalez-Longatt).

https://doi.org/10.1016/j.ijepes.2023.109560
Received 25 June 2023; Received in revised form 1 September 2023; Accepted 4 October 2023
Available online 14 October 2023

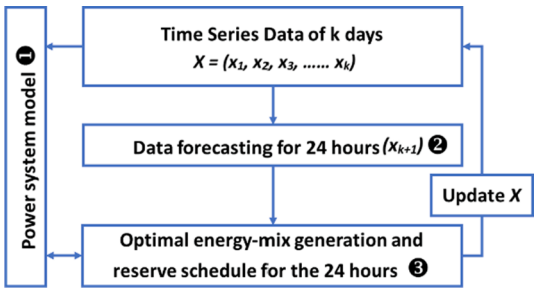

Fig. 1. An overview of the proposed methodology.

system [2]. Also, these RESs are of a stochastic nature, which may introduce complexities in the demand/supply chain within a power system. Introducing an efficient and sufficient reserve to the power system can be a good option to address the challenges of short-term demand/ supply unbalance because of the stochastic nature of RESs [8,9].

Research has been carried out in a variety of dimensions to address the issues of modern power systems caused by the growing penetration of RESs. Technological developments in components such as inverters, converters, controllers, and so on are the essential sectors that can contribute to the secure operation of the power system. In a similar vein, the operating principle and management features of revolving power systems can play major roles in addressing the issues. Researchers are developing a wide variety of ideas and strategies to address the issues that have been identified as being caused by the rapidly shifting topologies of grids and the incorporation of new technology. For example, research papers [9–12] looked at the management of power system security by using economic measurements and the look-ahead dispatch approach. A detailed recovery plan is considered in these papers that guarantees the security of the power system with a possible minimum cost. On the other hand, a method of dynamic rescheduling has been proposed by Zhao et al. [13] for the large roll-out of connected power infrastructure for plug-in electric vehicles operating in extreme conditions. During the rescheduling process, the authors examined the stochastic nature of wind energy and used a real-value and binary particle swarm optimization technique to design the outputs of the project. Ardakani et al. [14], presented a linear chance-constrained optimization-based approach that dispatches and reserves the energy/ power for a day-ahead electricity market so that the RES integrated grid achieves reliable and secure operating points against the contingencies. Differently, Tang et al. [15], presented a stochastic unit commitment model that explores the ability of battery energy storage systems (BESS) to provide grid services by combining energy and reserve markets. It is shown that this model solves the uncertainty of RESs and demand by analyzing BESSs and generators' reserves. Similarly, Zuo et al. [16], studied the performance of a low-inertial power system with grid-following (GFL) and grid-forming (GFM) power converters and a BESS. The authors of this study provided a model with a day-ahead scheduling layer to analyze daily system frequency containment using a day-long time-domain simulation.

While much of the existing literature has explored various dimensions of RES-integrated power systems, there's still a marked lack of focus on optimizing the day-ahead energy portfolio in grids largely dependent on converters, especially those that take advantage of real-time data from transmission system operators (TSOs). Previous studies often simplify the complexities of the grid, overlooking the subtleties of time-series data or failing to examine the coordinated interaction among diverse power-generating technologies in day-ahead planning. Additionally, there has been insufficient emphasis on the nuanced balance between cost factors—from energy production to system integrity—and grid stability. This paper seeks to address these gaps by harnessing detailed time-series data from the TSOs of the Nordic grid. It is aimed at a more dynamic, cost-effective, and reliable energy configuration that can serve as a practical guide for TSOs. It promotes the optimized use of renewables, contributing to climate mitigation through emission reduction. Concurrently, it is assumed to strengthen grid resilience, offering more dependable solutions for managing the fluctuating nature of renewable energy, a key consideration for climate adaptation. By spotlighting a grid with a high share of RES, this research sets the stage for designing power systems that are sustainable, resilient, and economically sound in a world increasingly faced with climate-induced challenges.

This paper deals with the estimation of the optimal day-ahead energy-mix proportion that would ensure the secure functioning of a power system dominated by converters. To accomplish this goal, this paper uses the time-series data that is accessible on a time-series basis from the TSOs of the Nordic countries. The time-series data is used to estimate the day-ahead values using a data-driven model, which is then utilized to determine the optimal scheduling of the power producers using a model of energy generation and reserve scheduling. Required constraints are taken into consideration during the process of determining the optimal mix of energy from different power-generating technologies (i.e., synchronous generator (SG), GFL, and GFM). The cost of the energy generated from different generators, including charging and discharging of the BESS, generator start-up and shut-down cost, energy reserve cost, and service cost toward system strength are the terms of the objective function. This is done in order to ensure that the secure operation of the power system can be guaranteed in accordance with the regulations of the Nordic TSOs. Throughout the contents, the major contributions of this paper are as follows:

(a) Propose a concept that takes the historical time-series data from the TSOs, estimates a day-long operation stage, and evaluates how securely the power system is operating on a daily basis. This study estimates the best energy-mix proportions for every 24 h utilizing time-series data of generation and consumption of the Nordic grid with a resolution of three minutes.
(b) Data-driven model has been used to forecast the day-ahead values of the parameters that should be required to identify the optimal energy-mix proportion. A long short-term memory (LSTM) network as the forecasting model has been used to achieve state-of-the-art results.
(c) In order to ensure the secure functioning of the system, a model for energy-mix operation and reserve scheduling is utilized. The terms of the objective function include the costs related to generation, operation, maintenance, and system strength.

The presented paper is organized with the following structure. It begins by providing a historical context and an overview of the issues that have surfaced as a result of the widespread adoption of PEC-based technologies in the power grid. The challenges faced by today's power systems, which are reliant on huge amounts of PEC technology, are briefly highlighted. The approaches and presumptions that are used are laid out in Section 2. The datasets and systems that are taken into consideration are also described in detail. In Section 3, the data-driven model has been described that is used for forecasting purposes. In Section 4, the results of the investigation are presented and then thoroughly examined. Finally, the conclusions have been discussed in Section 5.

2. Methodology and assumptions

This section's primary focus is on describing the approaches that are ultimately chosen, as well as the assumptions that are made. Fig. 1 provides a summary of the approaches that are taken into consideration. The approach contains a power system model 1, a data-driven forecasting model 2, and the optimal energy-mix generation and reserve schedule model 3. First, it comes with a model of the power system 1, all of the components of which have been detailed according to the grid standard. The real-world power system provided the source for the

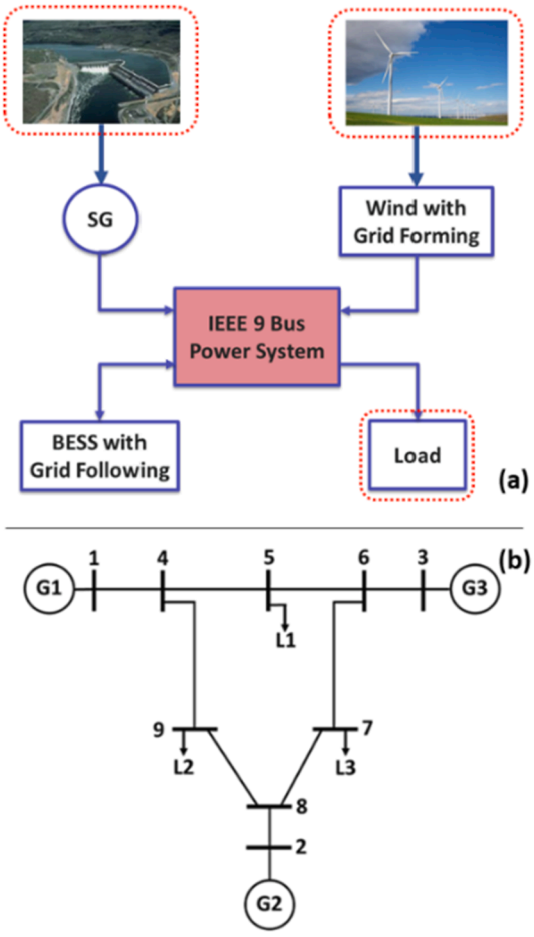

Fig. 2. (a) Overview of the considered system, and (b) Single line diagram of IEEE 9 bus system.

Table 1
Rating of the generators and the loads in the considered power system.

Parameters	Values
Generator 1	163 MW (1.025 pu) at 18 kV
Generator 2	72.19 MW (1.04 pu) at 16.5 kV
Generator 3	85 MW (1.025 pu) at 13.8 kV
Load 1	100 MW/ 35 MVAR
Load 2	125 MW/ 50 MVAR
Load 3	90 MW/ 30 MVAR

independent and variable time series data, which included parameters like power production and consumption. To begin, the time series data has been utilized to make an estimate of the values for the day ahead. The forecasting of the time series data for a day is done with the help of a data-driven forecasting model 2. The optimal scheduling of the power-generating technologies has been determined with an energy generation and reserve schedule model 3 after taking into account the constraints imposed by the power system as well as the time series data that is anticipated for the generation and consumption of power. The response of power-generating technologies such as SG, GFL, and GFM have been analyzed during optimal scheduling. An evaluation of the techno-economic impact is carried out while the appropriate distribution of the components is determined. It is also believed that the reserve schedule ensures the secure operation of the power system. All of these investigations have been conducted with MATLAB software, which contains both the simulation tools as well as the ANN features. The following sub-sections will provide a more in-depth discussion of each component and technique, including all of their particulars.

2.1. Power system components

As discussed in the previous section with Fig. 1, a standard power system model 1 is used to explore day-ahead scheduling with optimal energy-mix for the secure operation of a converter-dominated power system. This is conducted in order to find the best possible solution. The considered system's overview is depicted in Fig. 2(a). The IEEE 9 bus power system as shown in Fig. 2(b) is taken into consideration as the primary network. The rating of the generators and the load centers in the considered IEEE 9 bus power system are given in Table 1. It is also considered that the primary network operates at 230 kV and 50 Hz. Book by P.M. Anderson et al. [17] contains all of the information that is necessary to understand the power system model in further depth. During the course of the investigation, the authors made several assumptions, which can be shown in Fig. 2(a). It is assumed that the first generator is a SG, the second one is a BESS with a GFL, and the third generator contains a wind turbine with a GFM. In this particular investigation, both the dynamic properties of the generations and the load consumption are taken into consideration. The entirety of the system is created using MATLAB Simulink and the time domain is the simulation framework.

The model of the SG used in this study can be defined with Equations (1) and (2). Here in Equations (1) and (2), δ_i is the rotor angle in rad, ω_i is the shaft speed and ω_0 is the nominal speed in pu, H_i is the inertia constant in MJ/MVA, $P_{m,i}$ is the mechanical power, and D_i is the damping torque coefficient of i^{th} generator. The () sign indicates the derivative with respect to time. Similarly, r_a is the armature resistance, $v_{q,i}$ and $v_{d,i}$ represent the q-axis and d-axis components of the voltage, and $i_{q,i}$ and $i_{d,i}$ represent the q- and d-axis components of stator current [18].

$$\dot{\delta}_i = \omega_0(\omega_i - 1) \tag{1}$$

$$2H_i\omega_i\dot{\omega}_i = -D_i\omega_0(\omega_i - 1) + P_{m,i} - \left(v_{q,i}i_{q,i} + v_{d,i}i_{d,i} + r_a{i_{d,i}}^2 + r_a{i_{q,i}}^2\right) \tag{2}$$

Similarly, the grid-forming virtual emulator given in [19], is used as the GFM. A power electronic equipment called a GFM can vary the amplitude (i.e. magnitude and angle) of voltage and frequency at the Point of Common Coupling (PCC) [20,21]. GFM's major duty is to adjust the output voltage and/or current to keep the system frequency and voltage steady. A GFM can be considered as the slack-bus unit in an isolated energy system since it can inject instantaneous active and reactive power for frequency and voltage management [20,22]. It can be mathematically presented as (3) and (4) [19]. Here, ω_i and θ_i are the frequency and angle of voltage, and P_i is the active power generated by the i^{th} generator. Similarly, $\widetilde{m_i}$ and $\widetilde{d}_i$ are the positive values, known as virtual inertia constant and virtual damping constant.

$$\dot{\theta}_i = \omega_i \tag{3}$$

$$\dot{\omega}_i = -\widetilde{d}_i\,\omega_i - P_i \tag{4}$$

On the other side, GFLs operate as regulated current sources and use a phase-locked loop (PLL) to track the grid phase angle to keep the converters synced with the power grid [23]. In order to regulate the flow of current, one uses the observed phase angle. It regulates the active and reactive currents injected into the electrical grid to accomplish the desired power injection [24]. In the event of a power outage, the grid-following converter simply maintains the output current at the same level as before. However, it is unable to regulate the grid's frequency and voltage directly and must rely on either an additional voltage source or the grid itself [25]. The mathematical representation of the GFL can be presented as (5) and (6) [19].

$$\dot{\widehat{\theta}}_i = \widehat{\omega}_i \tag{5}$$

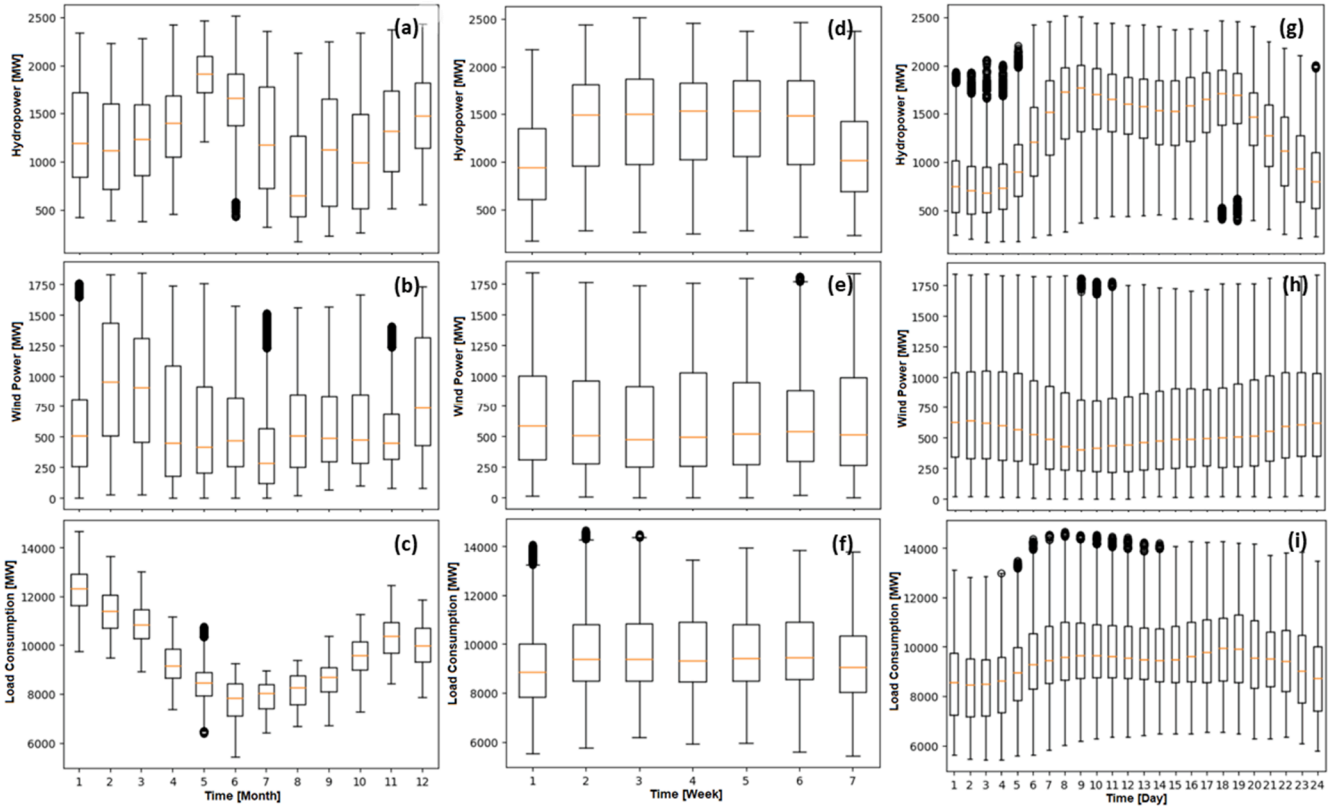

Fig. 3. Seasonal characteristics of the datasets for (a) monthly trend of hydropower, (b) monthly trend of wind power, (c) monthly trend of load consumption, (d) weekly trend of hydropower, (e) weekly trend of wind power, (f) weekly trend of load consumption, (g) daily trend of hydropower, (h) daily trend of wind power, and (i) daily trend of load consumption.

$$\tau_i \dot{\widehat{\omega}}_i = -\widehat{\omega}_i - K_{P,i} v_{q,i} - K_{I,i} \int v_{q,i} dt \tag{6}$$

Here, τ_i is the filter time constant, and $K_{P,i}$ and $K_{I,i}$ are proportional and integral gain constants of the component. Here in these Equations, the sign () indicates the estimated one.

2.2. Datasets

This analysis made use of real data for hydropower production, wind power production, and load consumption. The data are collected for the Nordic grid, and then they are scaled down in order to make them compatible with the IEEE 9 bus standard. Firstly, the data related to power generation and load consumption for the Nordic grid have been taken from the FINGRID TSO [26]. The data on hydropower production is taken from Finland and assumed that it is valid for all Nordic countries since the seasonal streamflow for different rivers from these countries seems to be in similar trends [27,28]. The data is collected throughout the year 2021, and their resolution is three minutes. After observing the raw datasets, it is identified that some of the datasets are not a number (NaN) type, and some seem to be coming from the wrong column. These observations provide a preliminary idea about the outliers within the collected datasets. For detailed investigation, the distribution of datasets is analyzed with the help of normal distribution (i.e., histogram). From the histogram, it is identified that the normal distribution of hydropower lies from minimum zero to a maximum of 3,688.96 MW. Similarly, the minimum and maximum values for wind power may vary from zero to 2,915.54 MW, and those values for load consumption may vary from 4,245.98 to 15,006.4 MW. The datasets that are outside of these limits are considered to be outliers. During the analysis, it is identified that, out of 174,988 samples, 763 outliers have been identified in the hydropower dataset, one in wind power, and 768 in the load consumption datasets. The identified outliers are then replaced with the mean values of the specific column (i.e., 944.27 for wind power, 1,609.8 for hydropower, and 9,668.44 for load consumption). It is believed that the new dataset reflects all of the qualities of the parameters, despite the fact that the data quality has been enhanced.

The seasonal pattern of the power generators from hydropower and wind power, as well as the load consumption, are evaluated for the purpose of providing a more in-depth understanding of the raw datasets. The box plots that display the monthly, weekly, and daily trend of the power-related parameters are shown in Fig. 3(a-i). It is clear from looking at Fig. 3(a-i) that the power production from wind and hydropower and the load consumption are subject to large amounts of variation. The wind profile is subject to random variation, and the load consumption is contingent on the nature of the consumer, which also exhibits a random nature. Hence, wind power generation and load consumption cannot be controlled, and it is independent. The trend of hydropower output, on the other hand, can be controlled to balance the supply–demand chain, and is considered to be dependent.

After the data have been preprocessed to get rid of any outliers, the data are next scaled down to comply with the requirements of the IEEE 9-bus standard. Normalization technique, as given in Equation (7) [29], is used to scale down the datasets so that the data can be achieved in the required form.

$$Z_i = \frac{X_i - \min(X)}{\max(X) - \min(X)} * Q \tag{7}$$

Here in Equation (7), X_i is the i^{th} value, $\max(X)$ is the maximum value and $\min(X)$ is the minimum value within the specific datasets. When performing the work of scaling down the data, the power rating of the power-generating technologies and the load consumption, as shown in Table 1, are used as maximum values Q that are needed for normalization. Also, the ratings of the power generators vary from zero to their

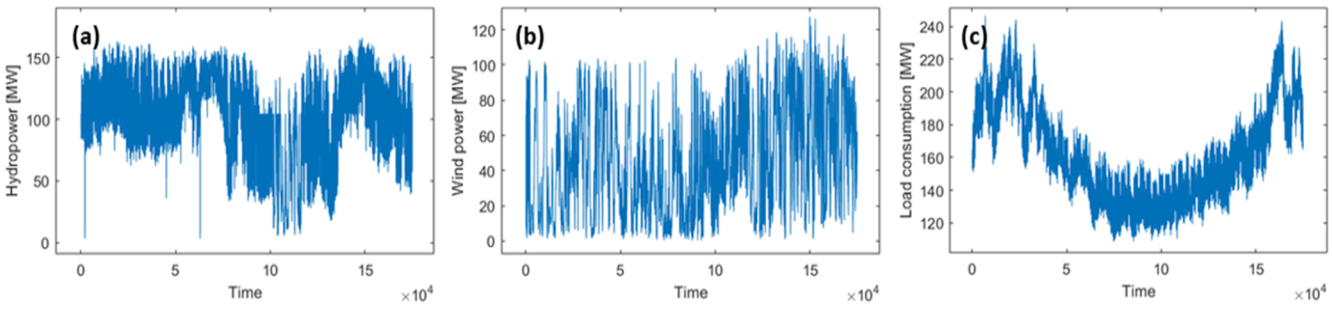

Fig. 4. Down-scaled profile of (a) hydropower, (b) wind power, and (c) load consumption (samples per unit of time).

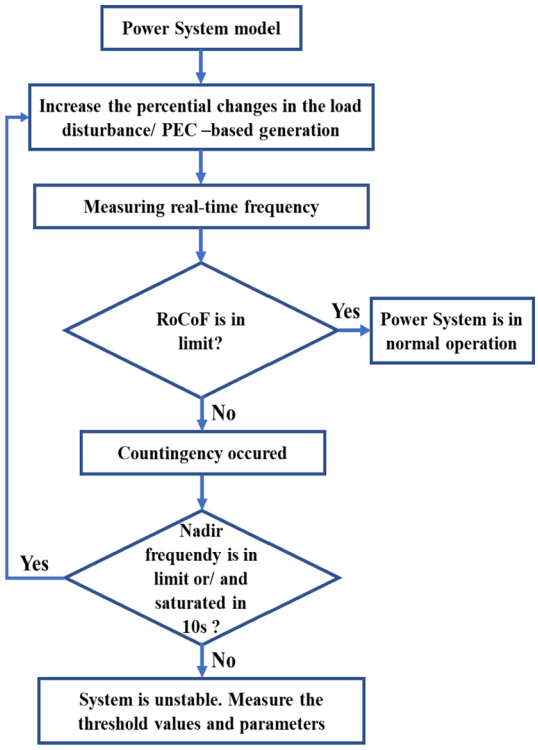

Fig. 5. Processes to determine the threshold values and secure function conditions for the considered power system model.

maximum values (as recorded in the datasets); $\max(X)$ is considered to be the maximum recorded value, whereas the $\min(X)$ is considered to be zero. Fig. 4 presents the characteristics of the scaled datasets, which are employed in this inquiry alongside the forecasting model 2 that provides the values for the parameters one day in advance (especially wind power and load consumption). A detailed description of the forecasting model 2 used in this study is presented in Section 3.

It is possible to consider the discharge of the water as a constant value for the entire day when analyzing the day-ahead estimation because hydropower production is entirely dependent on the flow of the water, and the flow of the water does not change significantly over short periods of time (assuming there are no significant changes in the weather, including rain). However, it is necessary to make frequent forecasts; monthly forecasting can be used for hydropower production. Whereas the nature of wind and the load consumption is stochastic; possibly perfect prediction is required while analyzing it. Hence, this paper highlighted the importance and mainly focused on the day-ahead forecasting of the two parameters: wind power production and load demand.

2.3. Energy-mix operation and reserve scheduling model for secure operation

As described in the introduction section, the main objective of this paper is to identify the optimal energy-mix proportion for the day-ahead operation of a RES-based power grid in a secure way. To identify the optimal proportion of the energy-generating technologies, the authors considered the cost as the objective function, which can be described by Equation (8). In this paper, four terms have been considered as the objective functions: (a) cost of the energy generated through different generators including charging and discharging of the BESS, (b) service charge provided by different power generators to maximize the power system strength, (c) generator start-up and shut-down cost, and (d) energy reserve cost.

$$\min \sum_{t\in\mathcal{T}} \left[\begin{array}{c} \sum_{g\in\mathcal{G}} \left(C^{p}_{g,t}\cdot p_{g,t} + C^{Up}_{g,t}\cdot u^{Up}_{g,t} + C^{Down}_{g,t}\cdot u^{Down}_{g,t} + C^{reserve}_{g,t}\cdot p^{reserve}_{g,t} \right) \\ + \sum_{e\in\mathcal{E}} \left(C^{Dis}_{e,t}\cdot p^{Dis}_{e,t} - C^{Charge}_{e,t}\cdot p^{Charge}_{e,t} \right) \end{array} \right] \tag{8}$$

Here in Equation, $C^{p}_{g,t}$, $C^{Up}_{g,t}$, $C^{Down}_{g,t}$, and $C^{reserve}_{g,t}$ are the cost parameters of the energy, generator start-up, generator shutdown, and reserve, respectively. Similarly, $C^{Dis}_{e,t}$ and $C^{Charge}_{e,t}$ are the cost parameters, whereas $p^{Dis}_{e,t}$ and $p^{Charge}_{e,t}$ are the energy supplied/ consumed while discharging and charging the BESS. $p_{g,t}$ and $p^{reserve}_{g,t}$ are generated energy by the generators at t time and the reserved energy. On the other hand, $u^{Up}_{g,t}$ and $u^{Down}_{g,t}$ are the unit variables that define the startup and shutdown of the generating units. Similarly, the $C^{p}_{g,t}$ is the cost parameters of the energy from different power producers, which are different for different power generators as per their resources and characteristics. For example, the cost of energy/ power generated through RESs is comparatively higher than that from non-renewable energy, since the community has allocated some incentive toward the RESs [30]. When we are talking about RESs, the SG comes as the first choice, since it is flexible to start and shut down, and also it can provide reliable supply and security toward the power system operation. On the other hand, introducing GFM/ virtual inertia is one of the best solutions that can support improving the system strength as well as power system stability. Similarly, BESS can be considered as a form of service provider for additional frequency service [31]. Hence, different energy/ power producer has different characteristics and their own role in the power system's quality, hence, it is most important to analyze the service cost for different generators carefully, while analyzing the cost functions. Equation (9) gives the distribution of the cost parameters for the generated energy, where $C^{gp}_{g,t}$ is the actual cost parameter for the generated energy from different generators, and C^{ss}_{g} is a cost parameter for the service provided by different generators to improve the system strength.

$$C^{p}_{g,t} = C^{gp}_{g,t} + C^{ss}_{g} \tag{9}$$

The idea of system strength is highly complicated and is still in the process of development; it is connected to the benefits of security,

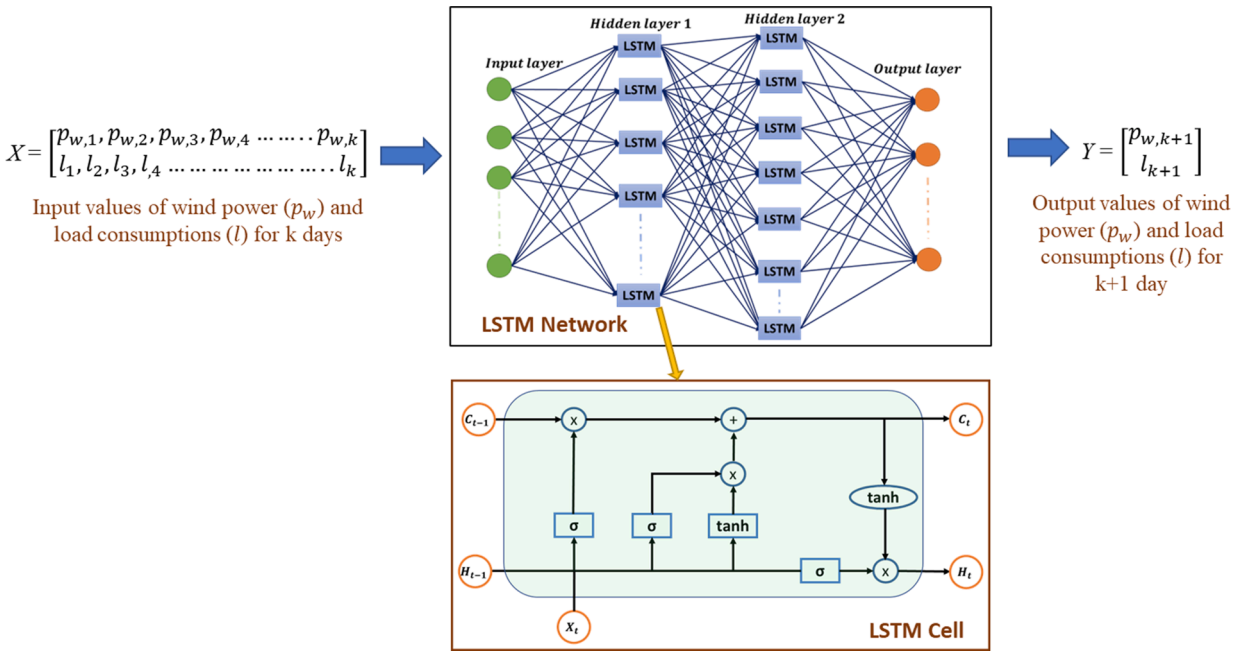

Fig. 6. Overview of the proposed model.

Table 2
Hyperparameters ranges/ types for tuning.

Parameters	Value/ types
Number of hidden layers	$\mathbb{Z}$[1,5]
Number of units in hidden layer	$\mathbb{Z}$[10, 200]
Activation function	[tanh, relu, sigmoid]
Learning rate	$\mathbb{R}$[0.00001, 1]
Dropout value	$\mathbb{R}$[0.1, 0.7]
L2 Regularization	$\mathbb{R}$[1e-10, 1e-2]

efficiency, and resiliency that the power system offers to consumers, participants, and investors [32]. In a simple sentence, the displacement of a SG within a power system decreases the system strength, but the increasing penetration should have a higher system strength level to operate the power system in a secure way. Even if the idea of system strength is not popular in the Nordic grid at the present time, this study makes an attempt to incorporate the cost associated with system strength into the calculation of the cost parameters. The idea of system strength is fairly common in Australia, and the Australian Energy Market Operator (AEMO) is responsible for determining the limit of system strength needs for the whole Australian electricity grid every five years [33]. After that, the local transmission network service providers (TNSP) are accountable for making and acquiring services to solve the system strength deficit in accordance with AEMO's directives. If the connection of generators that need system strength is the source of part of these costs being spent, then the generation in question should also share some of the costs associated with these services, as represented in the system strength mitigation requirement [34]. Hence, the cost related to system strength (i.e., C_g^{ss}) is also included in this study, which can be calculated by using Equation (10).

$$C_g^{ss} = C_{price}^{ss} \left(\frac{\$}{MVA}\right) \times LF^{ss} \times p_g^{ss}(MVA) \tag{10}$$

Here in Equation (10), C_{price}^{ss} is the system strength unit price, and the LF^{ss} is the system strength location factor; both factors are fixed by the authority every five years (especially for the Australian grid). Similarly, p_g^{ss} is the specified amount of system strength service, which is fixed at the stage of integration with the national grid. The cost parameters used in this paper are taken from regulations established by authorities from Australia, and the USA [35–37].

In order to optimize the cost function for the task at hand, certain constraints are taken into consideration. Equation (11) gives the relationship between the variables that are relevant to the in-operation, startup, and shutdown, while Equation (12) places constraints on the variables that are associated with the startup and the shutdown [16]. It is most important to be under a suitable range for the startup and

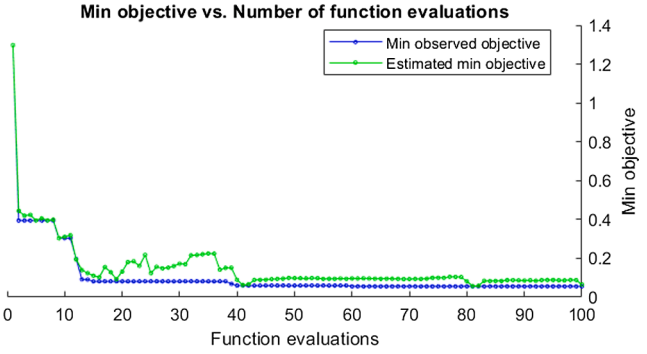

Fig. 7. Minimum objective vs. number of function evaluation.

Table 3
Hyperparameters for the presented LSTM model.

Parameters	Value/ types
Optimizer	Adam
Loss	MSE
Maximum Epoch	100
Mini batch size	32
Dropout value	0.5
Number of hidden layers	2
1st hidden layer	197 hidden units, tanh activation function, uniform initializer
2nd hidden layer	197 hidden units, sigmoid activation function, uniform initializer
Initial learning rate	0.001
Learn rate schedule	piecewise
L2 Regularization	0.00518
Input weight initializer	Glorot, with LR 1 and L2 factor 1
Recurrent weight initializer	Orthogonal, with LR 1 and L2 factor 1
Bias Initializer	Unit-forget-gate, with LR 1 and L2 factor 0

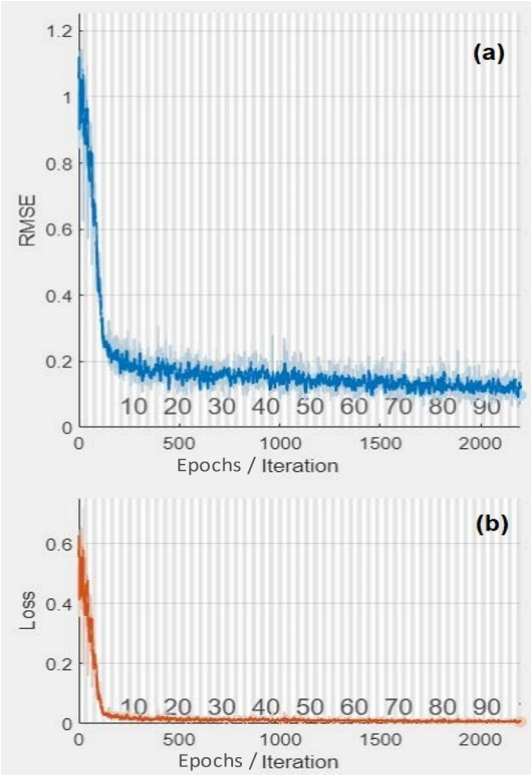

Fig. 8. Loss function with epochs/ iterations.

shutdown of the generators; the generators should follow the grid standards.

$$u_{g,t}^{on} - u_{g,t-1}^{on} = u_{g,t}^{Up} - u_{g,t}^{Down} \tag{11}$$

$$u_{g,t}^{Up} + u_{g,t}^{Down} \leq 1 \tag{12}$$

In a similar manner, Equation (13) [16], describes the link between the amount of energy generated by the generator and the maximum and minimum ramp rates at which the generators may operate, where $RP_{G,t}^{Up}$ and $RP_{G,t}^{Down}$ are the upper and lower bounds of the ramp rates, and $P_{G,t}$ is the power generated for the individual power-generating technologies at t. Ramp rate, also known as the maximum technical capability of a generating plant, is essentially the rating of power that can be changed each minute, and every country defines its values to manage its power systems. As an illustration, the Nordic TSOs' maximum ramping speed for flow changes is 30 MW/minute, while their maximum ramp changing rates for trading plans from one hour to the next are 600 MW.

$$u_{g,t}^{on} RP_{g,t}^{Down} \leq p_{g,t} - p_{g,t-1} \leq u_{g,t}^{on} RP_{g,t}^{Up} \tag{13}$$

Similarly, the constraint of the bound for the energy that should be reserved to give a sufficient supply is given in Equation (14) [16], where $P_G^{\min}$, $P_G^{\max}$, and $P_{G,t}^{reserve}$ are the minimum, maximum and available reserve bounds. The constraint for the phase angle stability is given in (15), where $\theta_G^{\min}$ and $\theta_G^{\max}$ are the minimum and maximum limits of the phase angle, and $(\theta_G - \theta_{SG})$ indicates the differences in the phase angles.

$$p_g^{\min} \leq p_{g,t} + p_{g,t}^{reserve} \leq p_g^{\max} \tag{14}$$

$$\theta_g^{\min} \leq \theta_g - \theta_{sg} \leq \theta_g^{\max} \tag{15}$$

Finally, the conditions for active power generation by all of the generators are given in Equation (16) [16]. In addition to this, it is considered that the BESS has not been discharged when the state of charge (SoC) becomes 30% or below, and no charging after the SoC becomes 99%.

$$u_{g,t}^{on} p_g^{\min} \leq p_{g,t} \leq u_{g,t}^{on} p_g^{\max} \tag{16}$$

One of the important factors used in this paper is system strength or system service cost, for which the system non-synchronous penetration (SNSP) ratio is considered as the metric. SNSP is the ratio of the real-time power generated through the non-SG and net HVDC interconnector import to total demand and HVDC interconnector export. It is mathematically expressed by Equation (17), and it provides a single constraint that encapsulates the issues of transient, voltage and frequency stabilities, and the consequences of transmission faults. Despite being an estimate, the measure has a reasonable real-time indication and can be used for operational as well as planning purposes [38].

$$SNSP\,(\%) = \frac{Non\ -\ Synchronous\ Generation\ +\ Net\ Interconnector\ Imports}{Demand\ +\ Net\ Interconnector\ Exports} \times 100 \tag{17}$$

However, the next objective of this paper is to identify the secure operating level of the power system; the authors simulated the power system model with a variety of plausible contingencies by increasing disturbances in load and PEC-based generation. In the worst credible scenario, generation dispatch is changed until the power system model is satisfied. From this condition, the SNSP ratio value is derived, indicating the power system's maximum SNSP ratio limit. Both the maximum threshold and secure functioning SNSP ratios are stated in percentage. Maximum threshold SNSP ratio and secure operational SNSP ratio are related by whichever credible contingency event has the largest influence on the rate of change of frequency (RoCoF) and frequency control. The detailed processes of getting these limits are given in Fig. 5.

3. Data-driven forecasting model

Data-driven model has been shown to be effective and is achieving a high level of accuracy in a variety of application fields, including medicine [39,40], agriculture [41,42], weather [43], power/energy systems [44–49], space [50,51], finance [52,53], and so on. Many ideas have gained widespread recognition, including feedforward networks, recurrent neural networks (RNNs), convolution neural networks (CNNs), and many others. Research articles [45–47,50,54–57] give a comparative review of artificial neural networks (ANNs) applicable to a variety of domains. Each one of them comes with a unique set of benefits and downsides. In this study, the authors adopted the Long Short-Term Memory (LSTM) network because of the following reasons: (a) handling long-term dependencies, (b) dealing with non-linear patterns, and (c)

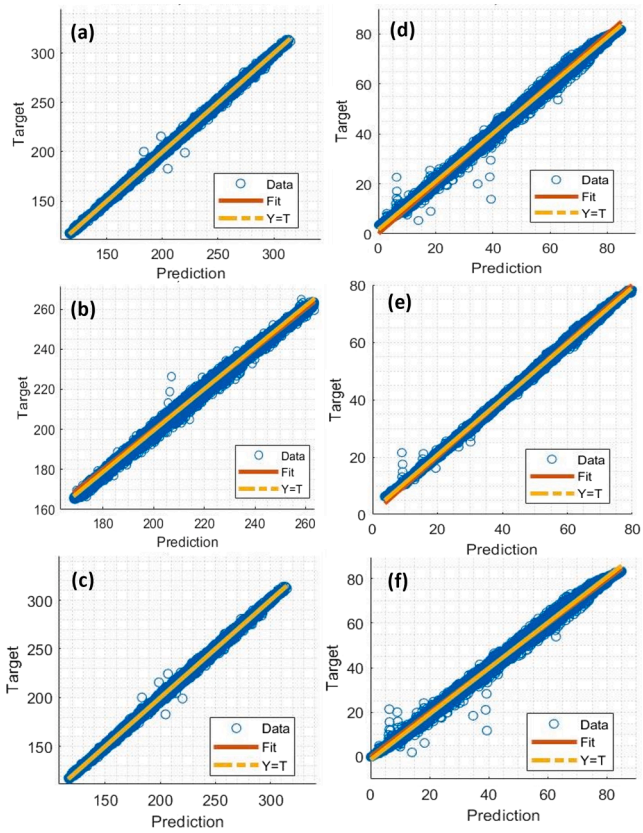

Fig. 9. Normalized regression of LSTM model for (a) load training data, (b) load testing data, (c) load all data, (d) wind training data, (e) wind testing data, and (f) wind all data.

robust to noise [58,59]. Because of the discussed characteristics, LSTMs are well-suited for time series forecasting, and they have been effectively employed in a wide variety of real-world problems including time series forecasting. As discussed in the introduction and methodology sections, the main objective of this paper is to estimate the day-ahead energy-mix proportions within a power system so that the power system can operate in a secure way. To obtain this objective, the power generations and load consumptions must be forecasted for the next 24 h, for which LSTMs could be a good option since it has all of the features that need to handle considered datasets and patterns of the outputs that are needed for further investigation.

LSTM is an expanded version of the RNN, which addresses the fundamental problem of having difficulties in learning long-term dependencies. In contrast to RNN, LSTM is equipped with a feature known as extended memory, which gives it the capacity to remember information for a longer time. The most significant improvement that has been made to the LSTM model is the inclusion of four gates, which are as follows: (a) input, (b) forget, (c) update, and (d) output. The forget gate determines whether the memory cell will be updated and controls how much information the current memory cell will receive from a potential new memory cell (19). On the other hand, the update gate determines whether the memory cell will be updated and determines how much information the current memory cell will receive from a memory cell from the previous step (20). Finally, the output gate is responsible for determining the values of the following hidden layer (21). [60]

$$\Gamma_i = \sigma\left(W_i\left[a^{\langle t-1\rangle}, X^{\langle t\rangle}\right] + b_i\right) \tag{18}$$

$$\Gamma_f = \sigma\left(W_f\left[a^{\langle t-1\rangle}, X^{\langle t\rangle}\right] + b_f\right) \tag{19}$$

$$\Gamma u = \tanh\left(W_u\left[a^{\langle t-1\rangle}, X^{\langle t\rangle}\right] + b_u\right) \tag{20}$$

$$\Gamma_0 = \sigma\left(W_0\left[a^{\langle t-1\rangle}, X^{\langle t\rangle}\right] + b_0\right) \tag{21}$$

Here in these Equations, W and b are the weight matrices and bias vectors of the recurrent network, a and X are the states of the neurons, and σ is the activation function. Using these four gates, the current state of the time-series model can be determined by using Equation (22), and the output can be calculated by using Equation (23). [60]

$$h_t = \tanh(W_{hh}h_{t-1} + W_{xh}x_t) \tag{22}$$

$$y_t = W_{hy}h_t \tag{23}$$

Going through detail, $h_t \in (-1,1)^h$ is the current state, h_{t-1} is the previous state, $y_t \in R^t$ is the output, $x_t \in R^t$ is the input, $W_{hh} \in R^{h*t}$ is the weight of the recurrent neuron, W_{xh} is the weight of the input neuron, W_{hy} is the weight of the output neuron, $b \in R^h$ is the bias vector parameters that need to be learned while model training. Fig. 6 presents the basic overview of the architecture of the LSTM model for the case of this study, where the main target is to forecast the day-ahead values of two variables; wind power and load consumption.

When performing analysis with a neural network, it is essential to have suitable values for several hyperparameters. The models' potential for performance-impacting learning behavior can be somewhat regulated by the hyperparameters, which play a role in this process. One of the most challenging aspects of utilizing data-driven models is determining which hyperparameters are appropriate to use. The selection of these hyperparameters can be difficult, and tuning them can take a significant amount of effort. As a consequence of this, the authors decided to utilize Bayesian optimization in order to locate the optimal values for the network hyperparameters. This methodology makes use of objective function evaluations in order to educate a Gaussian process model on the objective function that it keeps internally. For this optimization, the authors used the deep learning application provided by

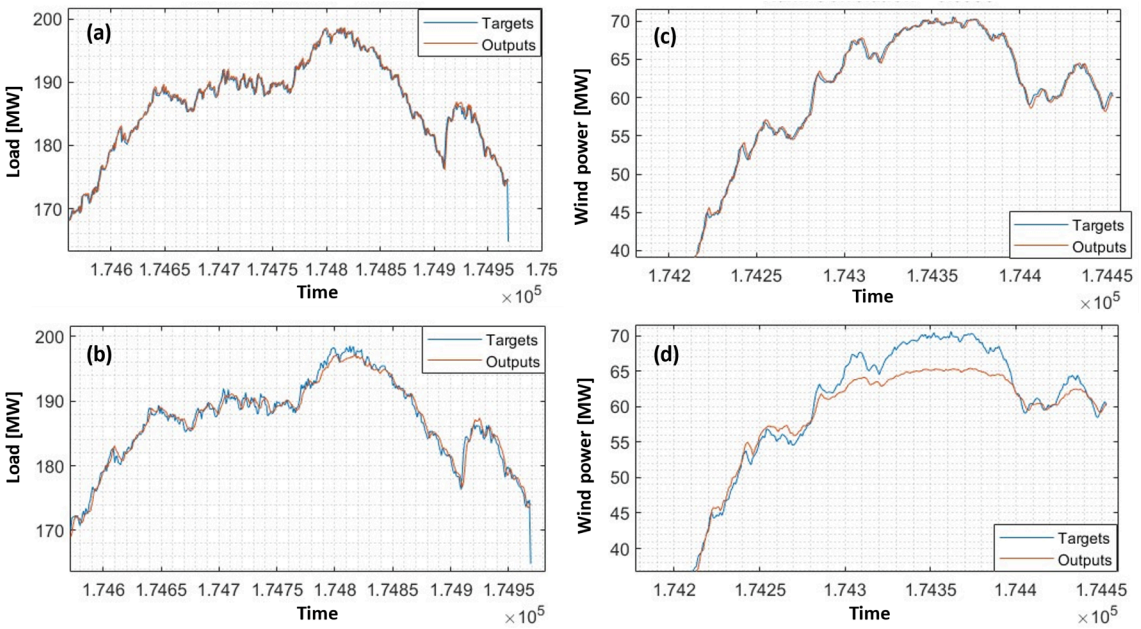

Fig. 10. Outputs (zoomed) for (a) load consumption with LSTM model, (b) load consumption with MLP model, (c) wind power with LSTM model, and (d) wind power with MLP model (samples per unit of time).

Table 4
Error indexes of the presented LSTM and MLP models.

Indexes	LSTM	MLP
MSE	0.0183	0.2125
RMSE	0.1352	0.4609
NRMSE	0.0046	0.0090

MATLAB software [61]. When tuning hyperparameters, a function known as *valErrorFun(optVars),* which is an optimization function, is taken into consideration. Different ranges for the other parameters have also been provided, which are listed in Table 2. Some of the most important characteristics to consider while designing the architecture of the model are the number of hidden layers and the number of neurons in each layer. On the other hand, the activation function plays an essential role in adding non-linearity and deciding which neuron should be engaged by computing the weighted sum and bias. In a manner comparable to this, the optimal learning rate might change based on the data provided and the network that is being trained. Similarly, the importance of regularization cannot be overstated when it comes to preventing both underfitting and overfitting. In order to facilitate the optimization processes, different potential values have been proposed, each of which takes into account the weight that each of these hyperparameters carries. Fig. 7 illustrates the relationship that exists between the minimal values of the objective function and the evaluation of the function whenever Bayesian optimization is used to determine the optimal values for the hyperparameters. When the simulation is run for a total of 100 epochs, as shown in Fig. 7, the observed and estimated values of the objective function come out to be 0.055348 and 0.0892, respectively. Based on the results provided by the Bayesian optimization, the important hyperparameters have been identified. The full list of the hyperparameters that are utilized for the presented LSTM model is given in Table 3.

Fig. 8 illustrates the errors of the model with epochs, which shows that the training performance of the model improves with the increase in the epoch or/ and iterations. The root mean square error (RMSE) is identified to be 0.1352 at the 100 epochs, whereas the loss function is calculated to be 0.0183. Both of the indicators seem to have decreased at starting in a significant amount, but the rate of change in the remaining parts is quite low, although the values are continuously decreasing. The authors decided to analyze the model for 100 epochs since the rate of change after that point is not significant; it changes at small rates. During the investigation of the performance of the presented model, the regressions of the model have been plotted for the training, testing, and all data sets for both wind power production and load consumption. All of these plots are given in Fig. 9. During the performance analysis of the presented model, the whole dataset has been divided into two sections: training (80%) and testing (20%). The data partitioning approach '*dataPartitioning(opt,data)*' is used to divide the datasets, which implements the gradient aggregation [62]. This is the case where the data on load consumption and wind power are utilized to make forecasts by utilizing the proposed model. The train-test split procedure is used to estimate the performance of algorithms when they are used to make predictions on data that was not used to train the model. The rank correlation values for all of the cases are identified as being higher than 0.980, which indicates the strength of the presented model.

For comparison, the authors also analyzed the datasets with next data-driven model namely, multilayer perceptron (MLP). Similar to LSTM, Bayesian optimization (i.e., trainbr) is used to find the hyperparameters for MLP. For MLP, it is identified that there are two feed-forward levels, with the layers consisting of eighty-nine neuron units. Other hyperparameters include the dropout value '0.2', the starting learning rate '0.005', learn rate schedule 'piecewise', linear regularization '0.00012', activation function 'sigmoid', optimizer 'adam', and so on. The results for power consumption by utilizing LSTM and MLP models are shown in Fig. 10 (a and b), while the outputs for wind power production within the power system are shown in Fig. 10 (c and d). The error indexes such as Mean Square Error (MSE), Root Mean Square Error (RMSE), and Normalized Root Mean Square Error (NRMSE) have been determined for both models and listed in Table 4. From these figures, the presented LSTM model appears to be a good fit for the datasets and the hyperparameters of the models that are being considered.

4. Result and discussion

Section 3 provides a comprehensive breakdown of the forecasting model and the values, whereas Section 2.1 looks into the specifics of the power system that is taken into consideration. Detailed descriptions of

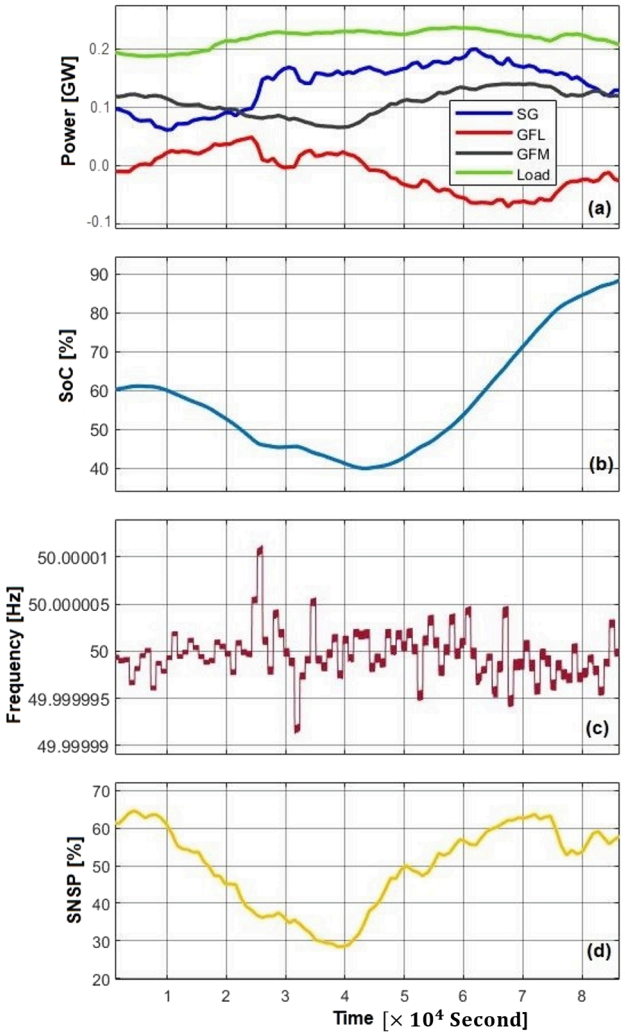

Fig. 11. (a) Power generated through generators, (b) SoC of BESS, (c) system frequency, and (d) SNSP values, for 24 h-time spans (samples per unit of time).

the data-driven model and the considered hyperparameters are discussed in Section 3. Whereas this section primarily centers around the results obtained from incorporating the day-ahead generation and consumption data into the dynamic model of the power system.

To begin with, the data-driven model estimates the variables of power generation and consumption for the next day. After that, these values are inputted into a dynamic model of the power system that includes an optimization model in order to arrive at a day-ahead optimal energy-mix proportion. It is assumed that the power system is supplied by a SG, wind turbines equipped with GFL, and BESS equipped with GFM in the condition that is being studied here. The optimal amounts of power that are supplied by and consumed by these components are shown in Fig. 11 (a). Here in Fig. 11 (a), when the value of the GFL is positive, the BESS is being discharged. When the value of the GFL is negative, the BESS is charged from the grid with the electricity generated by other generators. The SoC level of the BESS is presented in Fig. 11 (b) for the day ahead simulation scenario. It can be seen from looking at this figure that the minimum SoC that is recorded in this particular one-day simulation is 40 percent, which is well within the acceptable range of values. Similarly, Fig. 11 (c) illustrates the overall system frequency of the power system that is taken into consideration for this simulation model. Under these normal operating conditions, the frequency appears to be fluctuating with less variation, and it falls within the standard frequency limitations allocated by Nordic TSOs.

As discussed in subsection 2.3, the SNSP ratio is computed as the metric to use for the power system in the day-ahead scenario that is taken into consideration. Since the examined power system does not feature an HVDC exchange network, both the import and export values of the interconnector are taken to be zero for the sake of this paper's usual formulation, which is slightly different than Equation (17). It is identified that the SNSP ratio for the investigated situation ranges anywhere from 28% all the way up to 64%, as shown in Fig. 11 (d). These findings pertain to the normal functioning of the power system, where the maximum SNSP ratio is recognized as being 64%. Because of this, it can be assumed that the SNSP value of 64% is within a secure limit for running the power system that is being investigated.

There are certain ratings that apply to power-producing technologies while they are functioning under normal operating conditions. These ratings were taken into consideration when choosing the sizes for those technologies. Fig. 12 (a) illustrates the proportion of total installed capacity that is contributed by each of these three forms of power-generating technologies. In light of this consideration, the proposed model optimizes the power ratings of the technologies dynamically for the day-ahead scenario and allocates resources in accordance with these changes. Fig. 12 (b) depicts the hourly amount of energy supplied by each of these power-generating technologies for the analyzed day-ahead scenario.

However, the operation of the electrical system can be disturbed at any moment in time, and the power grid must be able to withstand that. A power system is susceptible to a wide variety of disturbances, each of which manifests itself in its own distinctive way. There are different types of faults, but some of the more prevalent ones are line-to-line faults, line-to-ground faults, multiple-line-to-ground faults, and so on [17]. Similarly, the sudden addition or subtraction of a large load or/and

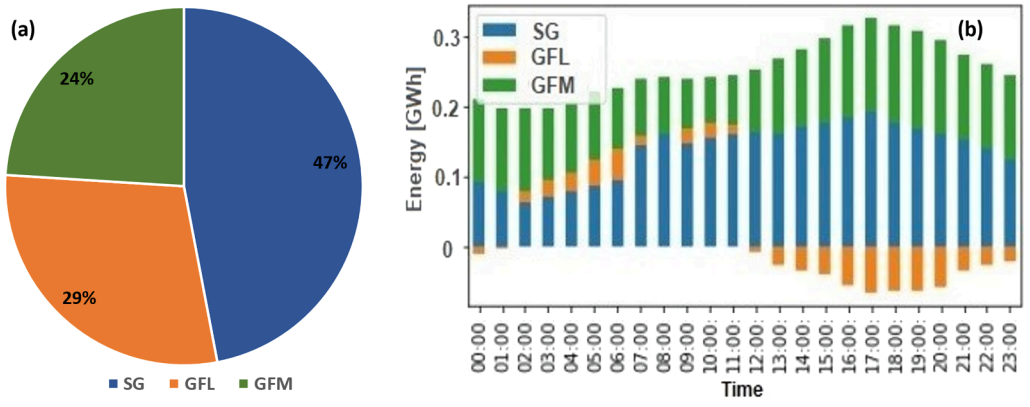

Fig. 12. Figure showing the (a) proportion of installed capacity, and (b) hourly generated electricity at the day-ahead scenario, for the power-generating technologies.

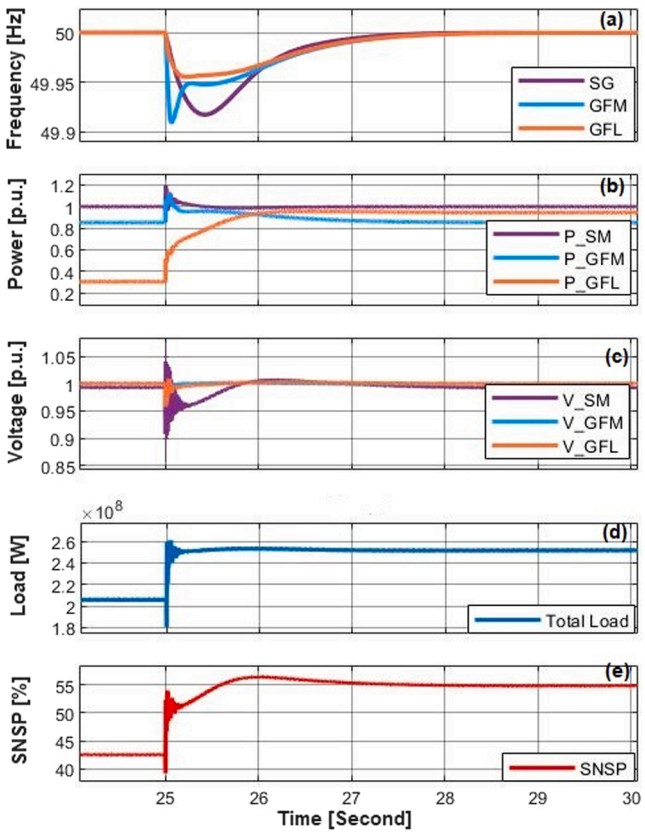

Fig. 13. System's responses (i.e., frequency, generation, voltage, load, and SNSP) at $\Delta P_L = 0.30$ pu.

power generation is considered a common disturbance in a power system, which can affect the performance of the overall power system. Therefore, it is essential to conduct a contingency analysis to evaluate the performance of the power system and ensure its security. Here in this paper, a disturbance is introduced into the model, and the responses to this disturbance have been evaluated using time-domain simulation. Fig. 13 provides a visual representation of the power system's parameters as they change in response to an increase in load of 30% (i.e., ΔP_L= 0.30 pu). As can be seen in Fig. 13, when a load is raised at the 25-second mark, the terminal voltages and frequencies of all generating units begin to decrease, albeit with some degree of variation. At the same time, they boosted their generation in order to fulfill the demand in a secure manner. This allowed for the demand to be met in a manner that was modified within a few seconds and maintained the system's stability. Because a 30% increase in load is significant, it takes a few seconds to maintain the saturation level. Similarly, the voltage level drops quite a bit farther at that precise moment. Nevertheless, within three seconds, most of the parameters achieve/ tend to achieve saturation, and they continue to supply the grid in a secure manner. In addition to that, before disturbance, the SNSP ratio for the considered power system seems to be 43%, whereas the value reached 57% when $\Delta P_L = 0.30$ pu is applied.

In order to conduct a comprehensive study, the level of load disturbance has been adjusted, and the maximum values of the SNSP ratio have been determined. The model of the power system is initially run under normal conditions, and then load disturbances are incorporated into the process. For analysis, different load disturbances are introduced, and the post-disturbance responses are observed. However, as soon as the disturbance reaches 38% of the total load, the system goes into an unstable state. This percentage is determined to be the technical limit of the load disturbance for the scenario that is being studied. The detailed processes of identifying this limit are given in Fig. 5. Fig. 14 displays the maximum SNSP ratio values that have been determined for each of these load disturbances. As shown in the figure, the SNSP ratio is observed to be 43% while operating under normal conditions, and it grows larger with each rise in the disturbance load ratings. The highest load disturbance that can happen while the power system is running in the mode being looked at is 38%, and this limit must be kept in order to keep things stable. It has been determined that the maximum SNSP ratio value for this stage is 59%, which can be considered the critical limit for power-generating technologies.

5. Conclusion

This paper presents a concept that utilizes historical time-series data from TSOs to estimate the day-long operation and evaluate the secure functioning of a power system on a daily basis. By leveraging the available datasets for the Nordic grid, the paper employs a data-driven model to forecast power generation and load consumption. Through the establishment of an energy-mix operation and reserve schedule model, this paper optimizes the selection of power-generating technologies and ensures sufficient reserves for secure system operation. Dynamic simulations, encompassing a 24-hour period and considering dynamic data on power generation and load consumption, are conducted to determine the optimal energy mix for the day ahead. Furthermore, contingency conditions are analyzed to assess the robustness of the power system model. Quantitative analysis, incorporating factors such as frequency, power generation, terminal voltages, and SNSP value, confirms the effectiveness of the proposed concept. Simulation results demonstrate that the considered power system can continue to operate securely even with an immediate 38% increase in total load, with a maximum SNSP value of 59%. While the highest SNSP value observed during normal operation is 64%, it exceeds 59% only for a brief period. Based on the low probability of encountering an immediate load increase of 38% together with an SNSP value exceeding 59%, it can be concluded that the power system is expected to function

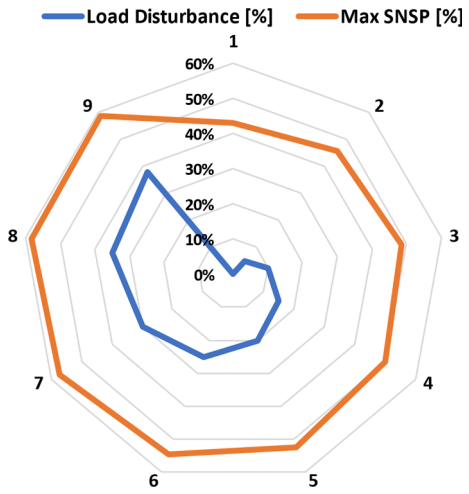

Fig. 14. Maximum SNSP ratio values at different load disturbance.

securely under various circumstances. This research contributes to climate change mitigation and decarbonization strategies by providing a reliable and sustainable approach to power system operation and management.

CRediT authorship contribution statement

Ashish Shrestha: Conceptualization, Formal analysis, Investigation, Methodology, Software, Visualization, Writing – original draft, Writing – review & editing. **Yaju Rajbhandari:** Formal analysis, Software, Visualization, Writing – original draft. **Francisco Gonzalez-Longatt:** Conceptualization, Supervision, Resources, Validation, Writing – original draft, Writing – review & editing.

Declaration of Competing Interest

The authors declare that they have no known competing financial interests or personal relationships that could have appeared to influence the work reported in this paper.

Data availability

Data will be made available on request.

Acknowledgment

Mr. Ashish Shrestha is thankful to the Department of Electrical Engineering, Information Technology and Cybernetics, University of South-Eastern Norway, Porsgrunn, Norway for the support that he receives during his PhD. Also, the authors are thankful to Prof. Nils-Olav Skeie, Assoc. Prof. Ru Yan, Assoc. Prof. Håkon Viumdal, Prof. Ola Marius Lysaker, Assoc. Prof. Ole Magnus Hamre Brastein, Assoc. Prof. Thomos Øyvang, Assoc. Prof. Nurilla Avozov, and Bishal Acharya for their support, suggestions, and motivation during the research period. This research work utilized the real data of Nordic grid for 2021 from FINGRID TSO; the authors would like to thank FINGRID for the datasets.

References

[1] Zappa W, Junginger M, van den Broek M. Is a 100% renewable European power system feasible by 2050? Appl Energy 2019;233:1027–50.
[2] Union, E.C.C.o.t.E. UN climate change conference (COP 26), World Leaders Summit, Glasgow, UK, 1 November 2021. 2021 11/11/2021]; Available from: https://www.consilium.europa.eu/en/meetings/international-summit/2021/11/01/#.
[3] Shrestha A, Ghimire B, Gonzalez-Longatt F. A Bayesian model to forecast the time series kinetic energy data for a power system. Energies 2021;14(11):3299.
[4] Shrestha A, Gonzalez-Longatt F. Frequency stability issues and research opportunities in converter dominated power system. Energies 2021;14(14):4184.
[5] Ju W, Sun K, Yao R. Simulation of cascading outages using a power-flow model considering frequency. IEEE Access 2018;6:37784–95.
[6] Shrestha A, Gonzalez-Longatt F. Parametric Sensitivity Analysis of Rotor Angle Stability Indicators. Energies 2021;14(16):5023.
[7] Shrestha A, Gonzalez-Longatt F. Parametric sensitivity analysis of rotor angle stability indicators: Simulation case. Energy Rep 2022;8:727–35.
[8] Khan S, Gawlik W, Palensky P. Reserve capability assessment considering correlated uncertainty in microgrid. IEEE Trans Sustainable Energy 2015;7(2):637–46.
[9] Gu Y, Xie L. Early detection and optimal corrective measures of power system insecurity in enhanced look-ahead dispatch. IEEE Trans Power Syst 2012;28(2):1297–307.
[10] Gu Y, Xie L. Stochastic look-ahead economic dispatch with variable generation resources. IEEE Trans Power Syst 2016;32(1):17–29.
[11] Tang C, et al. Look-ahead economic dispatch with adjustable confidence interval based on a truncated versatile distribution model for wind power. IEEE Trans Power Syst 2017;33(2):1755–67.
[12] Xie L, et al. Short-term spatio-temporal wind power forecast in robust look-ahead power system dispatch. IEEE Trans Smart Grid 2013;5(1):511–20.
[13] Zhao S, et al. A new power system active rescheduling method considering the dispatchable plug-in electric vehicles and intermittent renewable energies. Appl Energy 2022;314:118715.
[14] Ardakani FF, Mozafari SB, Soleymani S. Scheduling energy and spinning reserve based on linear chance constrained optimization for a wind integrated power system. Ain Shams Eng J 2022;13(3):101582.
[15] Tang Z, et al. Reserve model of energy storage in day-ahead joint energy and reserve markets: A stochastic UC solution. IEEE Trans Smart Grid 2020;12(1):372–82.
[16] Zuo Y, et al. Performance assessment of grid-forming and grid-following converter-interfaced battery energy storage systems on frequency regulation in low-inertia power grids. Sustainable Energy Grids Networks 2021;27:100496.
[17] Anderson PM, Fouad AA. Power system control and stability. John Wiley & Sons; 2008.
[18] Gibbard M, Vowles D. IEEE PES task force on benchmark systems for stability controls simplified 14-generator model of the south east Australian power system. South Australia: The University of Adelaide; 2014.
[19] Poolla BK, Groß D, Dörfler F. Placement and implementation of grid-forming and grid-following virtual inertia and fast frequency response. IEEE Trans Power Syst 2019;34(4):3035–46.
[20] Rocabert J, et al. Control of power converters in AC microgrids. IEEE Trans Power Electron 2012;27(11):4734–49.
[21] Paquette AD, et al. Sharing transient loads: Causes of unequal transient load sharing in islanded microgrid operation. IEEE Ind Appl Mag 2013;20(2):23–34.
[22] Paolone M, et al. Fundamentals of power systems modelling in the presence of converter-interfaced generation. Electr Pow Syst Res 2020;189:106811.
[23] Wang X, et al. Grid-synchronization stability of converter-based resources—An overview. IEEE Open J Industry Appl 2020;1:115–34.
[24] Gao X., et al. Grid-following and grid-forming control in power electronic based power systems: a comparative study. in IECON 2021–47th Annual Conference of the IEEE Industrial Electronics Society. 2021. IEEE.
[25] Du W, et al. Modeling of grid-forming and grid-following inverters for dynamic simulation of large-scale distribution systems. IEEE Trans Power Delivery 2020;36(4):2035–45.
[26] FINGRID, Kinetic energy of the Nordic power system- real time data. 2019.
[27] Ånund K. European hydropower capacity – a study of the correlation between the scandinavian and the alps hydropower system. Hydropower'05 - The Backbone of sustainable Energy Supply. Norway: Stavanger; 2005.
[28] EU, E., River Flow- Projected change in seasonal streamflow for twelve rivers, E.E. Agency, Editor.
[29] ZACH. How to Normalize Data Between 0 and 100. 2020; Available from: https://www.statology.org/normalize-data-between-0-and-100/.
[30] Gielen D, et al. The role of renewable energy in the global energy transformation. Energ Strat Rev 2019;24:38–50.
[31] Impram S, Nese SV, Oral B. Challenges of renewable energy penetration on power system flexibility: A survey. Energ Strat Rev 2020;31:100539.
[32] AEMO, NEM Engineering Framework. 2021, Australian Energy Market Operator.
[33] TransGrid, National Electricity Rules change proposal: Efficient management of system strength on the power system. 2020, Australian Energy Market Operator (AEMO): Australia.
[34] Yu L, et al. An overview of system strength challenges in Australia's National electricity market grid. Electronics 2022;11(2):224.
[35] Baringa; and DigSILENT, *Development of Renewable Energy Zones in the NEM*. 2020, Australian Renewable Energy Agency: Australia.
[36] Association, U.E.I., Levelized Costs of New Generation Resources in the Annual Energy Outlook 2022. 2022, US Energy Information Administration.
[37] (AER), A.E.R., Quarterly global FCAS prices by services. 2022: Australia.
[38] EirGrid S. System non-synchronous penetration definition and formulation. Ireland: Transmission System Operator; 2018.
[39] Shastri S, et al. Time series forecasting of Covid-19 using deep learning models: India-USA comparative case study. Chaos Solitons Fractals 2020;140:110227.
[40] Kaushik S, et al. AI in healthcare: time-series forecasting using statistical, neural, and ensemble architectures. Front Big Data 2020;3:4.
[41] Kurumatani K. Time series forecasting of agricultural product prices based on recurrent neural networks and its evaluation method. SN Appl Sci 2020;2(8):1–17.

[42] Guillén-Navarro MA, et al. A deep learning model to predict lower temperatures in agriculture. J Ambient Intell Smart Environ 2020;12(1):21–34.
[43] Gao Z., et al., Deep learning and the weather forecasting problem: Precipitation nowcasting. Deep Learning for the Earth Sciences: A Comprehensive Approach to Remote Sensing, Climate Science, and Geosciences, 2021: p. 218-239.
[44] Gasparin A, Lukovic S, Alippi C. Deep learning for time series forecasting: The electric load case. CAAI Trans Intelligence Technol 2022;7(1):1–25.
[45] Khodayar M, et al. Deep learning in power systems research: A review. CSEE J Power Energy Syst 2020;7(2):209–20.
[46] Ozcanli AK, Yaprakdal F, Baysal M. Deep learning methods and applications for electrical power systems: A comprehensive review. Int J Energy Res 2020;44(9):7136–57.
[47] Zhang Z, Zhang D, Qiu RC. Deep reinforcement learning for power system applications: An overview. CSEE J Power Energy Syst 2019;6(1):213–25.
[48] Rajbhandari Y, et al. Impact study of temperature on the time series electricity demand of urban nepal for short-term load forecasting. Appl Syst Innovat 2021;4(3):43.
[49] Gorostiza FS, Gonzalez-Longatt FM. Deep reinforcement learning-based controller for SOC management of multi-electrical energy storage system. IEEE Trans Smart Grid 2020;11(6):5039–50.
[50] Wang H, Raj B. A survey: Time travel in deep learning space: An introduction to deep learning models and how deep learning models evolved from the initial ideas. arXiv preprint arXiv:1510.04781, 2015.
[51] Saha S. et al., Deep learning for detecting multiple space-time action tubes in videos. arXiv preprint arXiv:1608.01529, 2016.
[52] Dingli A, Fournier KS. Financial time series forecasting-a deep learning approach. Int J Mach Learn Comput 2017;7(5):118–22.
[53] Lee SI, Yoo SJ. Multimodal deep learning for finance: integrating and forecasting international stock markets. J Supercomput 2020;76(10):8294–312.
[54] Torres JF, et al. Deep learning for time series forecasting: a survey. Big Data 2021;9(1):3–21.
[55] Brownlee J. Deep learning for time series forecasting: predict the future with MLPs, CNNs and LSTMs in Python. 2018: Machine Learning Mastery.
[56] Lim B, Zohren S. Time-series forecasting with deep learning: a survey. Phil Trans R Soc A 2021;379(2194):20200209.
[57] Lara-Benítez P, Carranza-García M, Riquelme JC. An experimental review on deep learning architectures for time series forecasting. Int J Neural Syst 2021;31(03):2130001.
[58] Wu Z, et al. A comprehensive review on deep learning approaches in wind forecasting applications. CAAI Trans Intelligence Technol 2022;7(2):129–43.
[59] Géron A. Hands-on machine learning with scikit-learn and tensorflow: Concepts. Tools, and Techniques to build intelligent systems; 2017.
[60] Staudemeyer RC, Morris ER. Understanding LSTM–a tutorial into long short-term memory recurrent neural networks. arXiv preprint arXiv:1909.09586, 2019.
[61] MATLAB. Deep Learning Using Bayesian Optimization. MathWorks/ MATLAB.
[62] Ma Y. et al., Adaptive Elastic Training for Sparse Deep Learning on Heterogeneous Multi-GPU Servers. arXiv preprint arXiv:2110.07029, 2021.